Bulletin of Mathematical Biology (2004) **66**, 1851–1873
doi:10.1016/j.bulm.2004.04.004

Cell Directional and Chemotaxis in Vascular Morphogenesis

D. AMBROSI AND A. GAMBA*

Dipartimento di Matematica,
Politecnico di Torino,
corso Duca degli Abruzzi 24,
10129 Torino,
Italy

E-mails: davide.ambrosi@polito.it; andrea.gamba@polito.it

G. SERINI

Division of Molecular Angiogenesis,
Institute for Cancer Research and Treatment,
10060 Candiolo,
Torino,
Italy

E-mail: guido.serini@ircc.it

In vertebrates, supply of oxygen and nutrients to tissues is carried out by the blood vascular system through capillary networks. Capillary patterns are closely mimicked by endothelial cells cultured on Matrigel, a preparation of basement membrane proteins. On the Matrigel surface, single randomly dispersed endothelial cells self-organize into vascular networks. The network is characterized by a typical length scale, which is independent of the initial mean density of deposed cells $\bar{n}$ over a wide range of values of $\bar{n}$. We give here a detailed description of a mathematical model of the process which is able to reproduce several qualitative and quantitative features of *in vitro* vascularization experiments. Cell matter is basically modelled as an elastic fluid subjected to a specific force field depending on the concentration of a chemoattractant factor. Starting from sparse initial data, mimicking the initial conditions realized in laboratory experiments, numerical solutions reproduce characteristic network structures, similar to observed ones, whose average size is theoretically related to the finite range of chemoattractant diffusion. A possible area of application of the model is the design of properly vascularized artificial tissues.

*Author to whom correspondence should be addressed.

0092-8240/04/061851 + 23 $30.00/0

1. INTRODUCTION

Understanding how blood vessels form in the organism has been a central issue in biomedical research during the last decade (Carmeliet, 2000). The self-assembly of endothelial cells into a vascular labyrinth is called vasculogenesis and is responsible for the early formation of blood vessels in the embryo. The process involves cell migration and is influenced by the presence of soluble molecules such as VEGF-A (vascular endothelial growth factor A) (Carmeliet, 2000; Helmlinger *et al*., 2000). *In vitro* assays have been devised in order to understand this basic morphogenetic process (Folkman and Haudenschild, 1980). Endothelial cells are cultured on a flat surface of Matrigel, a preparation which favours the formation of geometric tubular networks almost identical to capillary vascular beds observed *in vivo* (Kubota *et al*., 1988; Grant *et al*., 1989). Experiments show that these vascular structures are characterized by a typical length scale $\ell \simeq 200\ \mu$m, which is independent of the initial mean density $\bar{n}$ of deposed cells over a wide range of values of $\bar{n}$. This fundamental length scale has great physiological relevance, since typical intercapillary distances ranging from 50 to 300 μm have been known for a long time to be instrumental in effecting optimal metabolic exchange (Guyton and Hall, 2000). Varying the initial density $\bar{n}$, a percolative transition is observed: below a critical density n_c, several disconnected structures form, while connected structures are observed only for $\bar{n} > n_c$. When tracking the trajectory of single cells, most of them are seen to move towards regions of higher cellular concentration. Statistical analysis (Serini *et al*., 2003) indicates that the movement is mostly directed and that chemotactic effects should be considered.

The observation of experimental data raises several theoretical questions. How can separate individuals cooperate in the formation of coherent structures? Which is the mechanism regulating the pattern dimensions? A model introduced in a recent letter to study the percolation phenomenon (Gamba *et al*., 2003) proves able to give the answers to some of these questions. In this paper we provide a detailed mathematical deduction of the model and a thorough description of its properties and of its predictive potential. Our deduction is based on simple balance principles and on modelling assumptions suggested by experimental facts. The coupling of mass and momentum balance equations (enforced by specific bulk and surface forces) with a reaction–diffusion equation for a soluble growth factor provides a link between the scale of endothelial structures and the range of cell–cell interaction mediated by the release and absorption of soluble molecules. We describe the qualitative properties of the solutions of the model equations, thus providing an explanation for the mechanism of pattern formation. Many qualitative and quantitative features observed in the experiments, such as the value of the characteristic pattern size, are in very good agreement with those predicted by the mathematical model. As a matter of fact, the present model can be seen as a refinement of previously known chemotactic models taking into account the finite time for cell response to chemotactic gradients. The comparison is worked out in detail in

the text. Finally, since several observations contribute to the model validation, the model can be also used to perform computational experiments by varying parameters which are at the moment difficult to control in experiments. An example of this procedure is given in Section 6, where an application to the design of artificially grown vasculatures is proposed.

The model applies to the early stages of experiments of *in vitro* vasculogenesis performed with human umbilical-vein endothelial cells (HUVEC). We refer to Othmer and Stevens (1997) and the references therein for a general review of the mathematical literature on chemotaxis and to Velázquez (2002) for more achievements. The specific problem of vasculogenesis *in vitro* attracted specific attention following the work of Murray and Oster (1984), who first introduced a biomechanical model to explain pattern formation of bovine aortic endothelial cells. This approach has since then been extensively investigated by other authors (Ngwa and Maini, 1995; Manoussaki *et al*., 1996; Holmes and Sleeman, 2000). In the final section a critical comparison between these models and the approach proposed in this paper is carried out.

The structure of the paper is as follows. In Section 2 we review the experimental observations which provide the background for mathematical modelling. In Section 3 we show how, starting from very general assumptions extracted from experimental evidence, a continuum model of *in vitro* vasculogenesis experiments can be formulated. In Section 4 we describe the mechanism of pattern formation as qualitatively predicted by the model. In Section 5 we discuss the results of numerical simulations and the agreement of the model predictions with experimental data. In Section 6 we report the results of simulations performed in anisotropic conditions. Section 7 is devoted to a critical comparison between the proposed model and the relevant literature. In the conclusions section some open questions are illustrated.

2. Experimental Observations

In experiments, HUVECs are randomly seeded on Matrigel, a surface which favours cell motility and has biochemical characteristics similar to those of living tissues, and observed by time-lapse videomicroscopy for 15 h [Fig. 1(a)–1(e) and Serini *et al*. (2003)].

Main steps. The process of formation of a vascular-type network follows three main steps. (i) In the first step [3–6–9 h; Fig. 1(a)–1(c)], endothelial cells migrate independently, adhere with closest neighbours, and eventually form a continuous multicellular network [Fig. 1(d)] whose geometry is not substantially modified in the following steps. (ii) In the second step (6–9–12 h) the network just undergoes a slow deformation [Fig. 1(c)–1(e)], probably driven by a stress field generated by mutual traction, leaving the network topology essentially unaltered. (iii) Finally,

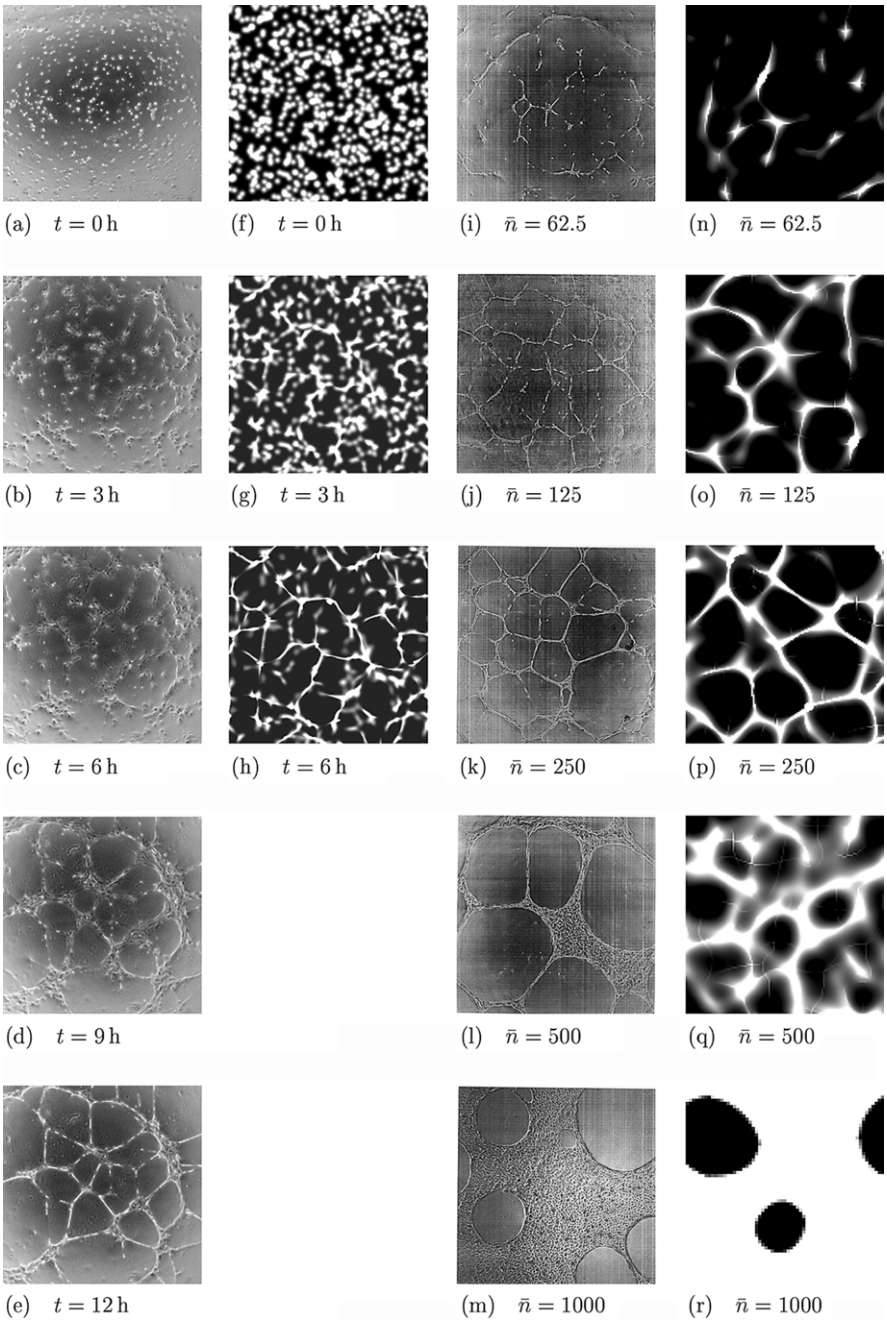

Figure 1. (a)–(e) The process of formation of vascular-type networks recorded by time-lapse videomicroscopy of a 4 mm^2 wide portion of Matrigel surface. (f)–(h) Time evolution resulting from a numerical simulation based on model (8)–(10). (i)–(m) Types of structures formed with varying number of cells over a 4 mm^2 area, as described in the text. (n)–(r) Results of numerical simulations obtained starting from the same initial density values as in (i)–(m).

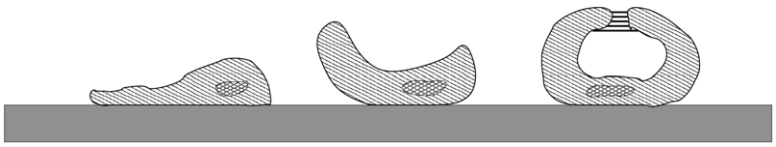

Figure 2. A schematic illustration of how single endothelial cells deposed on Matrigel fold up to form the section of a capillary-like tube.

in the third step, individual cells fold up to form capillary-like tubes [Figs. 1(e), 2] along the lines of the previously formed bidimensional network. The whole process takes 12–15 h to complete.

Chord length. The capillary-like network formed on Matrigel can be represented as a collection of nodes connected by chords [Fig. 3(a)]. The mean chord length measured for experimental records is approximately constant and equal to $\ell \simeq 200 \pm 20\ \mu$m over a range of values of $\bar{n}$ extending from 100 to 200 cells mm^{-2} [Fig. 3(b) and Serini *et al*. (2003)]. Since irregular structures produced from random initial deposition of endothelial cells are observed, only statistical measures of their geometrical properties are meaningful.

There are at least two methods available to measure the statistical distribution of chord lengths. A direct method consists of extracting from digitized images a graph structure by a computer assisted analysis and obtaining a database of chord lengths, which can then be analysed by statistical methods [Fig. 3(a)] and (Di Talia *et al*., in preparation). An alternative method consists of assigning a density function n_{ij} to each digitized record, where i, j are pixel coordinates and n_{ij} takes on the value 1 above a suitably chosen luminosity threshold, 0 below. One then computes the radial part of the density–density correlation function

$$P_{kl} = \sum_{ij} n_{ij} n_{i+l,\,j+k} \tag{1}$$

which for vascular-type networks shows a marked absolute minimum ℓ_0 [Fig. 8(a)] that can be taken as an alternative measure of the characteristic structure size. We checked that the two methods provide approximately equal results for the mean chord length of the relevant vascular-type structures.

Cell trajectories. Tracking of individual cell trajectories shows persistence in the direction of cell motion, with a small random component superimposed [Fig. 4 and Serini *et al*. (2003)]. In most cases the motion is apparently directed toward zones of higher concentration of cells. This suggests that a mechanism of cell cross-talk is present in the system. As a matter of fact, recent works (Carmeliet, 2000; Helmlinger *et al*., 2000) confirm that endothelial cells in the process of vascular network formation exchange signals by the release and absorption of VEGF-A. This growth factor can bind to specific receptors on the cell surface and induce

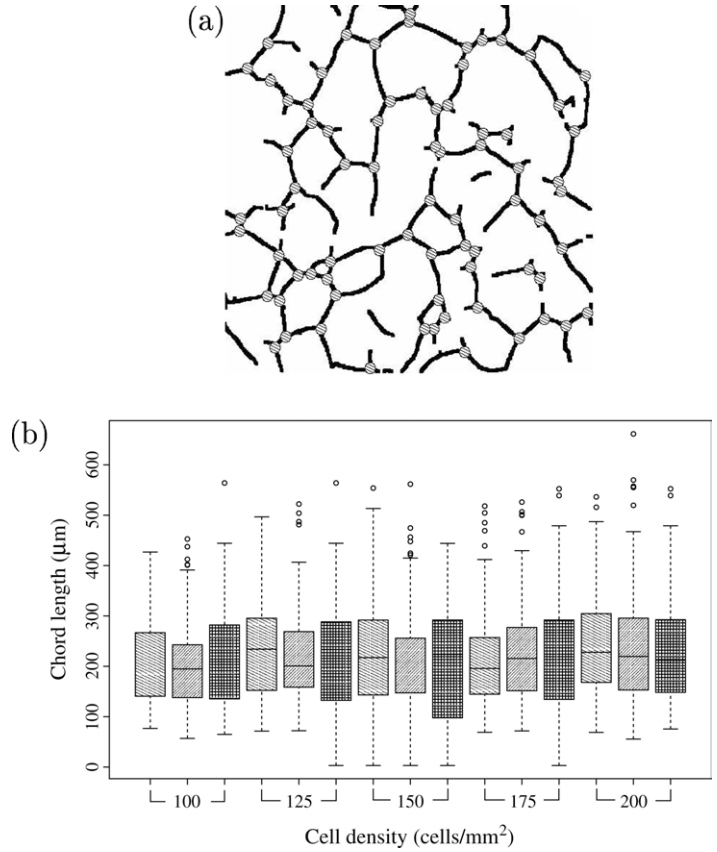

Figure 3. (a) Capillary networks are characterized by a typical graph structure, consisting of a collection of nodes connected by chords. (b) The statistical distribution of chord lengths of network structures obtained with varying initial cell densities and with cell samples taken from three different individuals (indicated with different shading patterns). Boxes show the median and the first and third quartile for a given cell density and sample. Whiskers extend to the most extreme data point which is no more than 1.5 times the interquartile range from the box. Circles denote outliers. The median chord length is essentially independent of the initial cell density and sample.

motion along its concentration gradients, a phenomenon known as chemotaxis (Othmer and Stevens, 1997). VEGF-A, like similar soluble molecules, is also known to be degraded by the environment in a finite time, mainly through oxidation processes (Gengrinovitch *et al*., 1999). Cell cross-talk through the exchange of soluble factors such as VEGF-A should thus be taken into account in a theory of vascular network formation. Experiments performed by extinguishing VEGF-A gradients with the addition of a saturating amount of VEGF-A show strong inhibition of network formation (Serini *et al*., 2003).

Accurate statistical analysis of the cell trajectories in normal and saturating conditions confirms the role of cell cross-talk. Velocity vectors can be measured from videomicroscopic records and two angles (ϕ and θ) can be computed, ϕ being

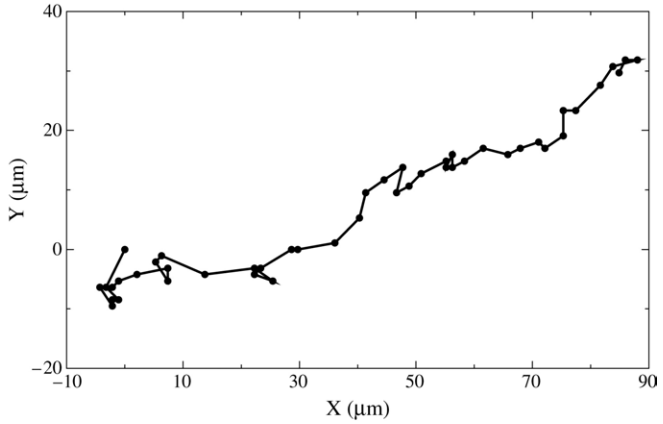

Figure 4. Tracking of a typical cell trajectory shows marked persistence in the direction of motion, with a small random component superimposed.

the angle between two velocities relative to the same trajectory, measured at subsequent intervals of time, and θ being the angle between velocities and simulated gradients of the concentration field at the same space point. Circular histograms [also known as Rose diagrams; see Mardia and Jupp (1999)] of ϕ, θ in both normal [Fig. 5(a)] and saturating conditions [Fig. 5(b)] are shown in Fig. 5. The Rose diagrams for ϕ, θ in normal conditions [Fig. 5(a)] show persistence of cell direction in time and alignment with the direction of simulated gradients of the concentration field. In saturating conditions [Fig. 5(b)], the Rose diagram for ϕ shows that cell movement maintains a certain degree of directional persistence, while the Rose diagram for θ shows that in saturating conditions the movement is completely decorrelated from the direction of simulated VEGF gradients.

Percolative transition. Fine tuning of an appropriate initial density $\bar{n}$ of deposed cells is mandatory for the proper development of vascular networks (Fong *et al.*, 1999). For this reason, experiments were performed with varying values of $\bar{n}$ (Gamba *et al.*, 2003; Serini *et al.*, 2003). This evidenced the presence of a percolative-like transition (Stauffer and Aharony, 1994). Below a critical value $n_c \sim 100$ cells mm^{-2} groups of disconnected structures [Fig. 1(i)] are formed instead of a single connected network. Around the critical value n_c [Fig. 1(j)] one observes the formation of a single connected network. At higher cell densities [Fig. 1(k)] the mean chord thickness grows to accommodate an increasing number of cells. Eventually, one observes a continuous carpet of cells interspersed with holes [the 'Swiss-cheese' pattern; Fig. 1(l) and 1(m)].

3. THE MATHEMATICAL MODEL

Starting from the experimental facts exposed in the preceding section a simple mathematical model of the *in vitro* vascularization process can be constructed.

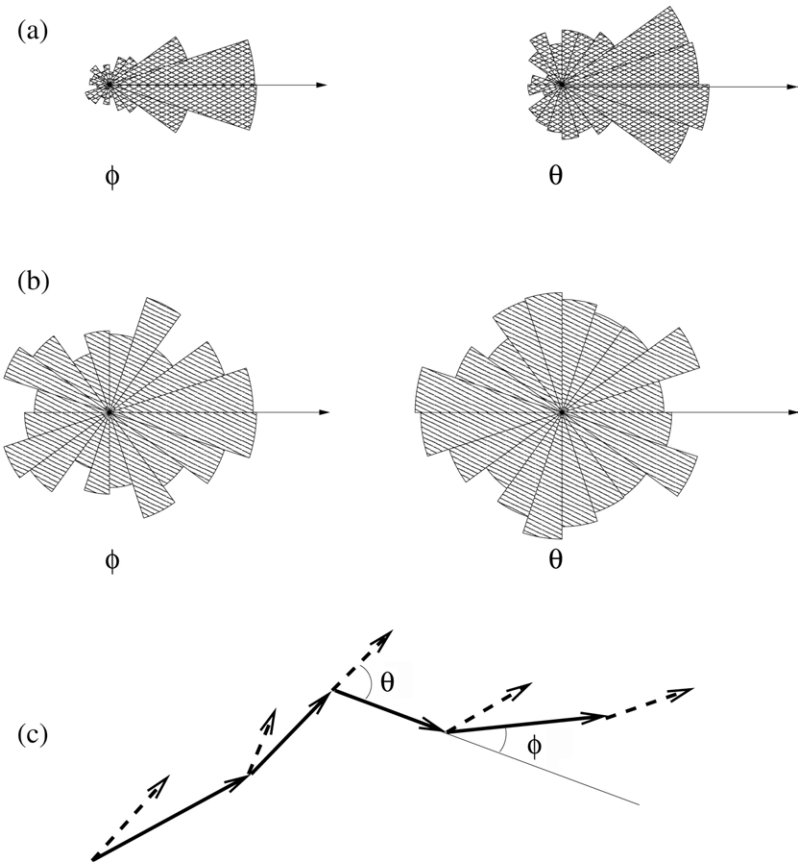

Figure 5. Rose diagrams (circular histograms) of ϕ, θ in normal conditions (a) and with a saturating amount of VEGF (b). The Rose diagrams for ϕ show that in saturating conditions also, cell movement maintains a certain degree of directional persistence. The Rose diagrams for θ show however that in saturating conditions the movement is completely decorrelated from the direction of the simulated VEGF gradients. (c) Definitions of angles ϕ, θ: solid arrows represent cell displacements; dashed arrows represent chemoattractant gradients.

Our guiding principle is not trying to formulate a maximally realistic model, which would contain many parameters difficult to determine experimentally, possibly characterized by a certain degree of randomness, but instead trying to provide the simplest possible model, characterized by a minimal set of measurable parameters, that is able to capture the main characteristics of pattern formation in the experimental conditions of interest. In this exposition we shall start therefore from very general hypotheses, necessary to describe cellular matter as a continuum subject to specific internal and external forces, and simple biological assumptions, suggested by experimental evidence. Once the main properties of the model are settled in the simplest possible case, a systematic activity of refinement becomes possible by the accurate modelling of other specific effects.

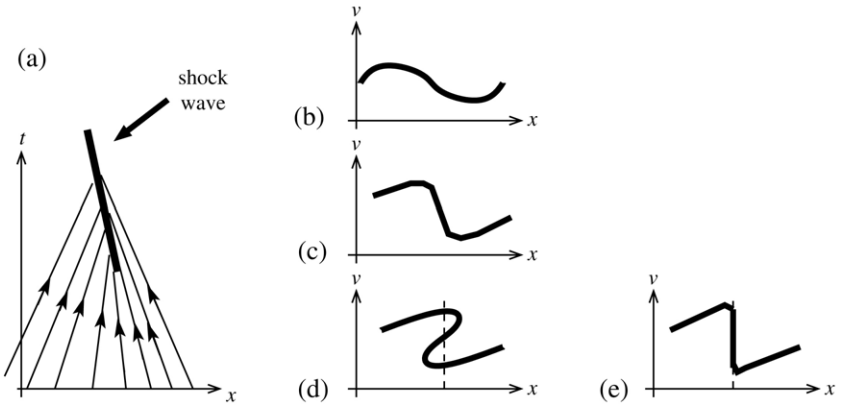

Figure 6. The schematic evolution of a velocity profile according to the one-dimensional Burgers equation. (a) The process of formation of a shock wave in world coordinates. (b, c) The process of formation of a shock wave in the single-particle phase space. (d) Formation of a multi-valued solution. (e) Viscous regularization of (d).

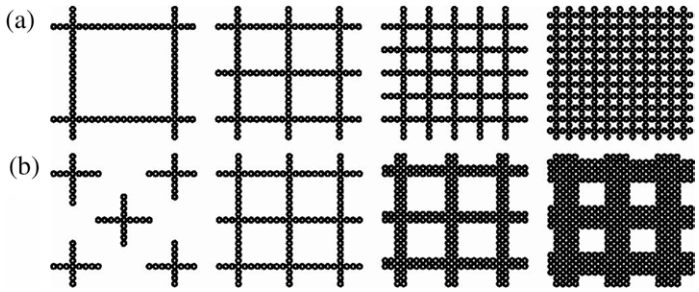

Figure 7. Different means of accommodating an increasing number of cells on a vascular-type network. (a) Without constraints on the average chord length; (b) imposing a constraint on the average chord length.

Since the major features of the observed geometric patterns are determined during the early stage described in Section 2, which takes place in the first hours of the experiment and is dominated by cell migration, the theoretical model focuses on the first step of network assembly. It should contain the main ingredients which are known from biological observation, such as cell migration and chemotaxis. It should also be able to reproduce some relevant facts, such as the existence of a typical chord length and the presence of a percolative transition.

Let us start from the following assumptions: it is possible to describe cellular matter by means of a continuous density field n and the corresponding velocity field $\mathbf{v}$. Let us consider a small element of area S on the Matrigel surface. In *in vitro* vascularization experiments proliferation is not observed, so the number of cells contained in an element of area S can change only because of flux through the boundary of S:

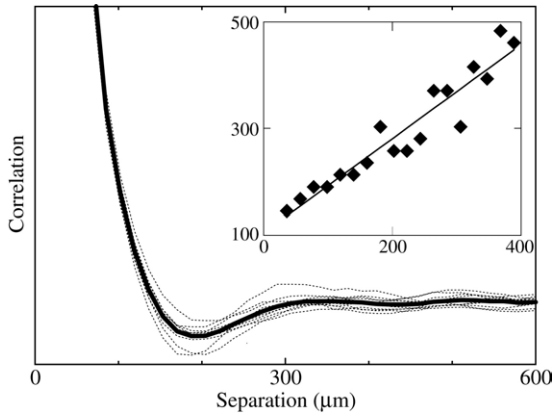

Figure 8. The radial part of the two-point correlator (arbitrary units) for simulated network structures with $x_0 = 100\ \mu$m. The thin lines correspond to ten different random realizations; the thick line is their average. The position of the absolute minimum of the thick line is l_0. Inset: a graph of l_0 versus x_0.

$$\frac{d}{dt}\int_S n d^2x + \int_{\partial S} n\mathbf{v}\cdot\mathbf{u}\, dl = 0, \tag{2}$$

where $\mathbf{u}$ is the outward normal to the boundary ∂S of the region S and dl is the line measure on ∂S. We also assume that cellular matter obeys a momentum balance law

$$\frac{d}{dt}\int_S n\mathbf{v} d^2x + \int_{\partial S} n\mathbf{v}(\mathbf{v}\cdot\mathbf{u})dl = \int_S n\mathbf{f}\, d^2x + \int_{\partial S} \mathbf{T}\,\mathbf{u}\, dl \tag{3}$$

where the second term on the l.h.s. represents the flux of momentum due to cellular matter flowing out of the area element S, $\mathbf{f}$ accounts for bulk (external) forces per unit mass acting on cellular matter, and the stress tensor $\mathbf{T}$ represents the internal (surface) forces.

Chemotactic forces. We make the hypothesis, based on biological evidence, that cells communicate through the release and absorption of molecules of a soluble growth factor, that can be reasonably identified with VEGF-A (Serini *et al.*, 2003). In this framework it is natural to introduce a chemotactic force per unit mass [see, e.g., Vasiev and Weijer (1999)]

$$\mathbf{f}_{\text{chem}} = \beta\nabla c \tag{4}$$

where c represents the concentration field of the chemical soluble factor and β measures the intensity of cell response per unit mass. On the basis of experimental evidence we assume that the chemotactic interaction has an attractive character ($\beta > 0$).

At a higher level of resolution in the description of biological reality one should also consider the concurrent action of inhibiting factors. The generalization of

the model to the case of multiple species of chemical factors, characterized by different physical properties and biological actions, will be described elsewhere (Di Talia *et al.*, in preparation). Here we will stick to the principle of extracting all the possible information from the simplest one-component model.

Dissipative interaction with the substratum. Another body force which is usually introduced in chemotactic models is the drag between cells and the substrate material. The simplest possible model for the dissipative interaction with the underlying substratum is given by the linear relation

$$\mathbf{f}_{\text{diss}} = -\gamma \mathbf{v} \tag{5}$$

where γ is a positive constant. It is worth noticing here that the combination of a driving force $\mathbf{f}_{\text{chem}}$ and a dissipative interaction $\mathbf{f}_{\text{diss}}$ allows one to model in a simple way a delayed response of the system to the chemotactic force. The fact that cells respond to chemoattractant cues with a finite time delay is sometimes neglected in mathematical models of chemotaxis, but is well known to biologists (see also the discussion in Section 7).

Limited compressibility of cellular matter. In order to model the fact that closely packed cells show a limited amount of resistance to compression we introduce a phenomenological, density dependent stress field acting only when cells become close enough to each other:

$$\mathbf{T} = -\varphi(n)\mathbf{I} \tag{6}$$

where $\mathbf{I}$ is the identity tensor and $\varphi(n)$ is zero below a critical density. In our simulations we experimented with several analytical forms of $\varphi(n)$ and found no relevant qualitative differences in the results as long as $\varphi(n) = 0$ for n below the close-packing density $n_0 = 1/2\pi r^{-2}$, where r is the average cell radius ($\simeq$20 μm), and $\varphi(n)$ is growing rapidly enough for $n > n_0$.

Diffusion of chemical factors. Chemical factors are assumed to be released by cells, diffuse in the surrounding medium, and degrade in a finite time. The process is simply modelled by a diffusion equation with a source and a degradation term:

$$\frac{\partial c}{\partial t} - D\Delta c = \alpha n - \tau^{-1} c, \tag{7}$$

where D is the diffusion coefficient, α the rate of release, and τ the half-life of the soluble mediator.

The mathematical model. By imposing that the balance laws (2) and (3) hold for any S and assuming that all the fields are smooth, we can deduce the differential

form of the balance equations. Then enforcing the constitutive relationships (4)–(7) we obtain the following differential model:

$$\frac{\partial n}{\partial t} + \nabla \cdot (n\mathbf{v}) = 0 \tag{8}$$

$$\frac{\partial \mathbf{v}}{\partial t} + (\mathbf{v} \cdot \nabla)\mathbf{v} = \beta \nabla c - \gamma \mathbf{v} - \frac{1}{n}\nabla \varphi(n) \tag{9}$$

$$\frac{\partial c}{\partial t} - D\Delta c = \alpha n - \frac{1}{\tau}c. \tag{10}$$

Equations (8)–(10) should be supplemented by initial and boundary conditions. In order to mimic the experimental setting we shall assume null initial velocities and assign $n(\mathbf{x}, t = 0)$ as a collection of N Gaussian bumps of width of the order of the average cell radius r, centred at random locations $\mathbf{x}_j$ distributed with uniform probability on a square of size L:

$$n(\mathbf{x}, t = 0) = \sum_{j=1}^{N} \frac{1}{2\pi r^2} \exp\left[-\frac{(\mathbf{x} - \mathbf{x}_j)^2}{2r^2}\right],$$

with periodic boundary conditions.

Further refinements. The model can be refined by taking into account some additional assumptions, which are not essential for the description of the self-assembly process but allow for a better mimicry of the biological system: (i) cells adhere when they come into contact; (ii) cell trajectories exhibit a small random component. Each of these assumptions can be implemented by the addition of a specific term in the r.h.s. of (9): (i) a diffusive term $\Delta\mathbf{v}$ dissipating kinetic energy in the proximity of developed structures; (ii) a small random noise term. Moreover, the phenomenological expressions (4)–(6) can be replaced by more detailed, possibly non-linear forms, in principle obtainable from *ad hoc* experiments. Although these refinements can in principle provide a more realistic mimicry of the *in vitro* experiments, they will not be considered here. Our opinion is that these refinements become relevant as soon as the new parameters that they introduce become measurable through specific experiments and are recognized as being responsible for observable new effects.

4. PROPERTIES OF THE MODEL

Characteristic scales. We chose to measure the cell density n in units of the close-packing density $n_0 = 1/(2\pi r^2)$; then, one can form three combinations from the

parameters appearing in equations (8)–(10), having the dimensions of a characteristic length, a characteristic time, and a characteristic concentration:

$$x_0 = \sqrt{D\tau}, \qquad t_0 = \sqrt{\frac{D}{\alpha\beta n_0}}, \qquad c_0 = \frac{n_0 \alpha L^2}{D}\xi^2 \tag{11}$$

where L has the dimensions of a length and $\xi = x_0/L$. We will later chose L to be the size of the computational box. The length x_0 is the effective range of chemical interaction among cells. This is easily understood thinking of a soluble molecule which is released by a cell, performs a random walk in the medium, and is degraded after a time τ. The time t_0 is linked to the characteristic time needed for structure formation, because of its relation to the chemotactic response through β. The concentration c_0 is a measure of the amount of soluble factor produced by a single cell during time τ.

Using the rescaling (11) the only (dimensionless) parameters left in (8)–(10) are ξ and $\gamma' = t_0\gamma$.

Pattern formation. In the absence of the pressure term, i.e., for low densities, cells tend to achieve the limit velocity $\mathbf{v} = (\beta/\gamma)\nabla c$ corresponding to the balance of chemotactic and drag force: in this limit one recovers traditional chemotactic models [see Othmer and Stevens (1997), Hillen and Othmer (2000), Othmer and Hillen (2002) and the discussion in Section 7]. In its general form, however, system (8) and (9) is a multidimensional inviscid Burgers equation with a forcing term (Burgers, 1974; Shandarin and Zeldovich, 1989; Gurbatov *et al*., 1991; Vergassola *et al*., 1994). In one spatial dimension, the Burgers equation is well known for developing highly organized spatial structures starting from generic initial conditions. The mathematical mechanism is as follows. The equation describes the motion of a fluid of non-interacting particles which perform uniform motions according to their initial velocities. During time evolution, faster particles catch up with slower ones. In this way, initial inhomogeneities in the velocity profile [Fig. 6(b)] are amplified by the dynamics [Fig. 6(c)] and, in the absence of viscosity, lead to multi-valued solutions [Fig. 6(d)], corresponding to faster particles overrunning the slower ones. A viscous term $\nu\Delta\mathbf{v}$, where ν represents kinematic viscosity, prevents multi-valuedness and one observes instead the formation of a set of shock waves of finite width [Fig. 6(a) and 6(e)], where most of the matter concentrates.

Since the formation of network structures is a generic property of the Burgers equation, arising from the simple dynamics of a fluid of particles which interact and adhere only when they come into close contact, it is to be expected that it will be preserved even in the presence of the forcing term $\beta\nabla c$. Moreover, the presence in the r.h.s. of (9) of the density dependent pressure term should not substantially modify the dynamics during the first step of pattern formation. Pressure becomes

relevant in the presence of high densities, i.e., in the proximity of formed structures, and contributes to their regularization. However, in our biological model the regularization and remodelling of formed patterns takes place in a new regime (which we identified in Section 2 as the 'second step' of pattern formation), which probably requires the use of an *ad hoc* viscoelastic model.

Coupling with chemical mediators. Let us now consider the information encoded in the coupling of the continuum model (8) and (9) with the diffusion equation (10). This can be understood in the simplest way if we neglect pressure and assume for a moment that diffusion is a faster process than pattern formation ($\tau^* \ll 1$), so that the dynamics of c is 'slaved' to the dynamics of n and the derivative term $\partial c/\partial t$ can be neglected in a first approximation. Then it is possible to solve (10) formally for c and to substitute in (9), thus obtaining

$$\frac{\partial \mathbf{v}}{\partial t} + (\mathbf{v}\cdot\nabla)\mathbf{v} = \frac{1}{n_0 t_0^2}\nabla(x_0^{-2} - \Delta)^{-1} n. \tag{12}$$

The appearance in the dynamical equations of the characteristic length

$$x_0 = \sqrt{D\tau} \tag{13}$$

suggests that the dynamics could favour patterns characterized by this length scale. As a matter of fact, if we rewrite the r.h.s. of (12) in Fourier space as

$$\frac{1}{n_0 t_0^2}\frac{\mathrm{i}\mathbf{k}}{k^2 + x_0^{-2}} n_{\mathbf{k}}$$

we observe that the operator $\mathrm{i}\mathbf{k}/(k^2 + x_0^{-2})$ acts as a filter, which selects the Fourier components of n having wavenumbers of order x_0^{-2}, damping the components with higher and smaller wavenumbers.

One then has the following scenario: initially, non-zero velocities are built up by the gradient term ∇c due to the presence of random inhomogeneities in the density distribution. Then, chemoattraction amplifies the inhomogeneities and forms a capillary-like network. Density inhomogeneities are translated in a landscape of concentration of soluble factors where details of scales $\lesssim x_0$ are averaged out by the action of the non-local operator in the r.h.s. of (12). Particles start moving toward the crests of the landscape, which are separated by valleys of width $\sim x_0$. In this way, the model provides a most direct link between the dimension of the structures and the range of intercellular interaction. We remark that the arguments above do not necessarily rely on the identification of the chemoattractant agent c with VEGF-A: other soluble growth factors could provide intercellular communication leaving the whole theory unaltered.

Percolation. The concept of percolation has been used in statistical mechanics to describe the formation of connected clusters of randomly occupied sites in systems close to critical values of the parameters. By varying the occupation probability in infinite systems one observes a phase transition in which the probability of percolating over a connected cluster extending across the whole system suddenly jumps from 0 to 1 (Stauffer and Aharony, 1994). Percolative transitions have been thoroughly investigated and are classified in a small number of 'universality classes', characterized by scaling laws with well defined 'critical exponents'. These exponents are fingerprints of the growth process that led to vascular structure formation and it has been suggested that they may help in discriminating between healthy and pathological structures (Gazit *et al.*, 1995).

The presence of a percolative-like transition in the formation of vascular networks (Gamba *et al.*, 2003) is by no means obvious, and is linked to the average constancy of the chord length. As a matter of fact, there are at least two ways of accommodating an increasing number of cells on a vascular-type network. The first one [Fig. 7(a)] is allowing arbitrary chord lengths: in this case connected clusters can be formed, at least in principle and in an infinite system, starting from arbitrarily low cell densities. Alternatively [Fig. 7(b)], one can impose a constraint on the chord length, but then for low densities only sets of disconnected clusters can be observed. From our analysis, it appears that Nature in this case chose the second way. This can be explained by observing that widely spaced capillary networks, such as the one on the left of Fig. 7(a), would not be able to perform their main function, i.e., to supply oxygen and nutrients to tissues (Guyton and Hall, 2000). This confirms that there must exist a precise mechanism controlling the average chord length during vascular formation, such as the one hypothesized in the deduction of model (8)–(10).

5. NUMERICAL SIMULATIONS

Numerical simulations of the model have been performed discretizing the system of equations (8)–(10) on squares of 256^2 and 512^2 equispaced nodes with periodic boundary conditions. A finite volume conservative scheme of Godunov type (LeVeque, 1990) has been used for the hyperbolic part of the equations (i.e., transport and pressure), while a spectral approach has been used for the r.h.s. of (10).

The simulations have been performed using the dimensionless form of (8)–(10) obtained by the rescaling (11). In this way, the only adjustable parameters left are $\gamma' = t_0\gamma$ and $\xi = x_0/L$ (see Tables 1 and 2). Simulated network structures have been observed not to depend on γ' for values $<10^2$ (only the needed machine time varied). The computational time has been mapped to real time by assuming $t_0 = 6$ h, the characteristic time of network formation in the experiments. The computational box has been mapped to the area observed by the microscope by choosing $L = 2$ mm. The parameter $\xi = x_0/L$ has been set to 0.1 in order to fit

Table 1. Experimental parameters.

Parameter	Value	Comment
D	10^{-7} cm s^{-2}	Diffusion coefficient of VEGF in the medium (Walter *et al.*, 1992; Muller *et al.*, 1997; Pluen *et al.*, 1999)
τ	64 min	VEGF half-life (Serini *et al.*, 2003)
r	20 μm	Cell radius (Serini *et al.*, 2003)
t_0	6 h	Characteristic time of structure formation in the experiments (Serini *et al.*, 2003)

Table 2. Computational parameters.

Parameter	Value	Comment
ξ	0.1	Fitted in order to reproduce the observed value of the average chord length. This value corresponds to an interaction radius $x_0 \simeq 200$ μm, in good agreement with the experimental value for $\sqrt{D\tau}$.
φ_0	10^{-4}	Values of this order correctly reproduce the 'Swiss cheese' structure observed for high density values.
γ'	0–10^2	Observed structures appear not to depend on γ' for values chosen in this range.

the experimentally observed chord length (see below). This corresponds to a value $x_0 \simeq 200$ μm, in approximate agreement with the experimental value of $\sqrt{D\tau}$ (see below). For the pressure function, the following form was used:

$$\varphi(n) = 0 \qquad \text{for } n \leq n_0, \qquad \varphi(n) = \frac{L^2 n_0 \varphi_0}{t_0}\left(\frac{n}{n_0} - 1\right)^3 \qquad \text{for } n > n_0$$

with $\varphi_0 = 10^{-4}$. We have observed that a large variation is allowed in the choice of φ_0 and even in the functional form of $\varphi(n)$, as long as two properties are satisfied: (i) $\varphi(n)$ is null for $n < n_0$, and (ii) it is monotonically increasing for $n > n_0$.

Simulations and experiments are in remarkable agreement (Fig. 1). The experimentally observed percolative transition is correctly reproduced: by varying the initial number of cells one switches from a phase in which several disconnected structures are formed to a phase in which a single connected structure appears [Fig. 1(i)–1(r)]. The introduction of the pressure term described allows one to reproduce also the transition to the 'Swiss-cheese' regime experimentally observed for $\bar{n} \gtrsim 300$ cells mm^{-2} [Fig. 1(m) and 1(r)].

In order to obtain an objective measure of the characteristic structure size for the results of numerical simulations one can apply the method described in Section 2. The radial part of the density–density correlator

$$P(\mathbf{x}) = \int n(\mathbf{y}) n(\mathbf{y} + \mathbf{x}) d^2 y \tag{14}$$

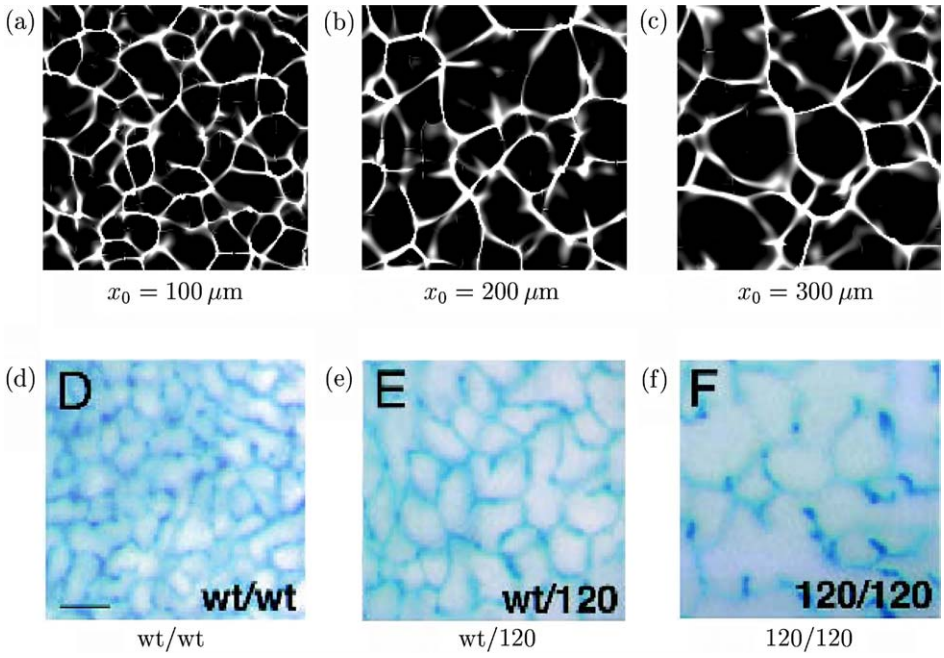

Figure 9. (a)–(c) Results of simulations of system (8)–(10) with the same set of initial conditions and three different values of the chemical interaction radius x_0. (e), (f) Figures reproduced by kind permission of the publisher from Ruhrberg *et al*. (2002), showing murine vascular networks. Vascular networks formed in mice (wt/120 and 120/120) lacking heparin-binding isoforms of VEGF-A form vascular networks with a larger mesh then those formed in wild-type mice (wt/wt).

of mature structures, averaged over many realizations of the random initial conditions, shows a marked absolute minimum $\ell_0 \simeq \bar{\ell}$ (Fig. 8), where $\bar{\ell}$ is the direct measure of the average chord length. Plotting ℓ_0 versus ξ, an approximate linear relation with a slope of order 1 (Fig. 8, inset) is obtained, confirming the qualitative argument exposed in Section 4.

Thus the model predicts that the diffusivity and the half-life time of the chemoattractant directly control the size of the vascular structure. Intriguingly, this seems to be in agreement with the observation that mice lacking heparin-binding isoforms of VEGF-A, characterized by smaller diffusivity, form vascular networks with a larger mesh [Ruhrberg *et al*. (2002) and Fig. 9]. Although the vascular patterns observed *in vivo* in Ruhrberg *et al*. (2002) are mainly thought to be generated by angiogenesis rather than vasculogenesis, one cannot exclude the possibility of a simultaneous occurrence of the two phenomena (Cleaver and Krieg, 1998).

The theoretical prediction (13) about the characteristic length of vascular structures can be compared with experimental data. The diffusion coefficient for major angiogenic growth factors can be estimated from available data of molecular radii (Walter *et al*., 1992; Muller *et al*., 1997) using the Einstein–Stokes relation $D = k_B T/(6\pi\eta r_H)$ where k_B is Boltzmann's constant, T the temperature, η the solvent

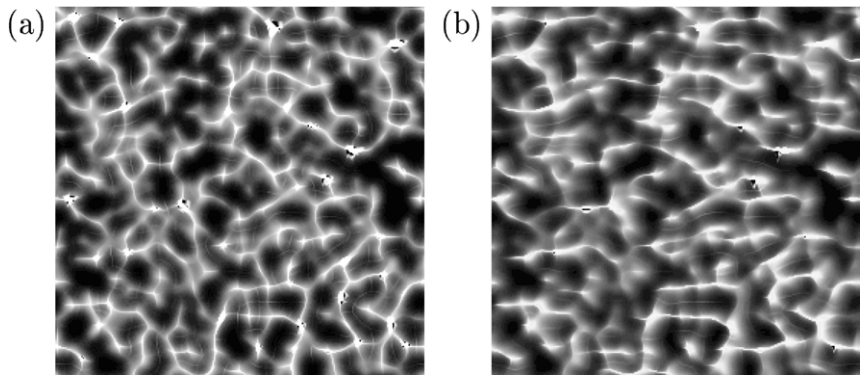

Figure 10. Simulation of the formation of vascular structures (a) in normal conditions and (b) under an imposed stream of $u_0 = 0.5 \times 10^{-4}$ cm s^{-1}, starting from the same initial conditions at time $t = 0$.

viscosity, r_H the hydrodynamic radius of the molecule (Pluen *et al.*, 1999). This gives $D \sim 10^{-7}$ cm^2 s^{-1}. The measurement of the half-life of VEGF-A in our experimental setting was done using a radioactive tracer, giving $\tau = 64 \pm 7$ min (Gamba *et al.*, 2003; Serini *et al.*, 2003). This yields $x_0 \sim 100$ μm, which is in good agreement with the experimental data.

6. Vasculogenesis in Anisotropic Conditions

Tissue engineering is one of the hottest medical frontiers of the new millennium. A relevant difficulty, hampering current efforts to gain robust results, is obtaining properly organized vascular networks, suitable for metabolic exchange in ischaemic tissue (Richardson *et al.*, 2001). The insight gained from the mathematical model (8)–(10) suggests that suitably distributed chemoattractant concentrations could be used to control the geometry of artificially grown vasculatures[†]. A simple way to control the form of artificial vasculatures could be to use microscopic flows of the liquid medium which carries the chemoattractant substances. While such experiments are difficult to realize at the moment, one can easily attempt to predict the result by just adding a transport term in equations (8)–(10). In the simplest case, one can consider adding a constant (in time and space) velocity field $\mathbf{u}_0$ in the balance equation for the chemoattractant agent:

$$\frac{\partial c}{\partial t} + \nabla \cdot (\mathbf{u}_0 c) - D\Delta c = \alpha n - \frac{1}{\tau} c. \tag{15}$$

The results are shown in Fig. 10, where mature structures with and without superimposed flow are compared. The superposed transport field is horizontally directed with magnitude $u_0 = 0.5 \times 10^{-4}$ cm s^{-1}, corresponding to a Peclet number $Pe = 5$ ($Pe = u_0 \xi / D$). One can observe that transport modifies patterns which

[†]We thank P. Netti for having drawn this point to our attention.

now exhibit an anisotropic structure: some vertical chords have disappeared; some new vertical ones form and stretch. The time necessary for the morphogenesis process is about 25% larger than that without transport. Generally speaking, the pattern is more disordered, a tendency that grows with the Peclet number (not shown).

The above described experimental conditions are probably realizable with existing techniques. An experiment conducted along these lines could be an interesting 'proof of principle' for model (8)–(10). More generally, one could think of ways to produce in the laboratory concentration distributions of chemoattractant characterized by particular geometries. Model (8)–(10) could be used to predict the form of the resulting vascular network.

7. Discussion of the Results

In order to compare system (8)–(10) to existing chemotactic models, let us assume that the inertia term $d\mathbf{v}/dt = \partial\mathbf{v}\partial t + (\mathbf{v}\cdot\nabla)\mathbf{v}$ is much smaller than the friction term $\gamma\mathbf{v}$, so that (9) gives $\mathbf{v} \simeq \gamma^{-1}(\beta\nabla c - n^{-1}\nabla\varphi)$. Substituting into the mass conservation equation (8) gives

$$\frac{\partial n}{\partial t} - \frac{1}{\gamma}\nabla^2\varphi(n) = -\frac{\beta}{\gamma}\nabla\cdot(n\nabla c). \tag{16}$$

Assuming moreover $\varphi(n) = n$, this gives, together with the diffusion equation (10), the classical Keller and Segel model (1970). This model is known to be able to produce patterns characterized by isolated clusters [see, e.g., Velázquez (2002)], but not network-like clusters of the kind described here. The essential difference from model (8)–(10) lies in the presence of the 'inertial' term $d\mathbf{v}/dt$ in equation (9). This term models a delay in the cell response to the chemotactic cue, a phenomenon which is known to biologists as a particular form of directional persistence (Serini *et al.*, 2003). Ignoring this delay implies instantaneous alignment of cell velocities with the chemoattractant gradients. Model (8)–(10) can be seen therefore as a refinement of classical chemotactic models, taking into account a finite time of cell response to varying chemoattractant gradients. It is an interesting fact that the consideration of this effect leads to peculiar qualitative properties of the solutions such as the appearance of network-like patterns.

The mathematical model introduced in the previous sections is obtained by first imposing the balance laws for the quantities of interest (cell density and momentum, concentration of chemoattractant), and then providing the constitutive relationships necessary to close the problem (namely the nature of the force fields). This procedure is typical of continuum mechanics, and has been often used in biomathematics; we just mention Vasiev and Weijer (1999), who used a two-component chemotactic force in a fluid-mechanical model of *Dictyostelium discoideum* mound formation, Ambrosi and Preziosi (2002) and Byrne *et al*. (2003), who adopt the formalism of porous media to describe the mixture of cell and intercellular liquid.

Referring in particular to vasculogenesis, Murray and Oster (1984) proposed a similar approach to experiments with bovine aortic endothelial cells (BAEC) carried out by Vernon *et al*. (1992). According to these authors, in the experiments, cells stretch to self-organize into a network in a time of the order of 20 h. This behaviour has been translated into a mechanical model where the Matrigel surface is assumed to behave as a linear viscoelastic material deformed by traction forces exerted by cells (Murray and Oster, 1984; Ngwa and Maini, 1995; Manoussaki *et al*., 1996; Holmes and Sleeman, 2000). The absence of a free-migration regime reported by Vernon *et al*. (1992) is the main difference from the experiments discussed here, that refer to the early stages of *in vitro* vasculogenesis performed with human umbilical-vein endothelial cells (HUVEC). From a biological point of view, migration and traction can be considered as different programs that an individual cell is able to execute. One can argue that the start of either program is dictated by the environment, e.g., by the fact that the cell is isolated or among a closely packed group of other cells. So, different initial conditions can put the system either in a migrating or in a viscoelastic regime, thus explaining the different observed phenomenologies.

From a mathematical point of view, a model which is biologically acceptable should also ensure that a stable steady state can be reached, at least for some set of parameters. This issue is strictly related to the question of the functional form of the pressure $\varphi(n)$, that in a stationary state should stably equilibrate the chemotactic forces. This point is currently under study.

8. CONCLUSIONS

Experiments on *in vitro* vasculogenesis on Matrigel have shown the existence of a fundamental scale characterizing vascular structures, and of a percolative transition between a disconnected vascular phase for low cell densities and a connected vascular phase for high cell densities. A continuum model has been derived from simple principles, based on the biological observation that endothelial cell migration and cross-talk are relevant factors in the morphogenetic process. The model provides a mechanism linking the range of interaction mediated by soluble growth factors to the structure dimensions. It reproduces with good accuracy the dynamics of the morphogenetic process, the observed scale of vascular structures, and the percolative transition.

The model suggests that endothelial cells self-assemble according to simple mathematical laws, which ultimately govern the vascular network geometry. One could even speculate that capillary structures may have evolved as a simple consequence of fundamental abilities of specific cell populations, such as motility, adhesion, and the ability to respond to chemical gradients.

The model predicts that the diffusivity and the half-lifetime of the chemoattractant determine the size of the vascular structure [Fig. 9(a)–9(c)]. Intriguingly, this agrees with *in vivo* observations by Ruhrberg *et al*. (2002) [Fig. 9(d) and 9(e)].

However, further work is needed to correctly understand in this case the respective roles of angiogenesis and vasculogenesis.

Comparing the results of experiments and computer simulations, some critical parameters which regulate the geometry of vascular networks were identified, such as endothelial cell density and the range of chemical interaction. This could be relevant to the engineering of properly vascularized, artificial tissues. The identification of key parameters controlling vasculogenesis could pave the way to tissue engineering approaches aimed at producing functionally vascularized organs. The numerical results described in Section 6 suggest how model (8)–(10) could be used to predict the form of vasculatures obtained via properly designed flows of chemoattractant factors.

A further interesting point is the following: anatomical and physiological evidence shows that the small capillary wall is constituted by a single folded endothelial cell; thus vascular networks having minimal chord thickness are in some sense optimal (Guyton and Hall, 2000). Such networks are obtained in a right neighbourhood of the percolative transition. This is an intriguing fact, since it connects a fundamental characteristic of a vital process with a very peculiar physical condition. One could wonder whether this is an isolated fact or whether other similar examples could be found. Moreover, in our *in vitro* assays the relevant critical parameter $\bar{n}$ is tuned by the experimenter. A natural question would be to ask how the system is self-tuned close to criticality in living beings, as in the embryo.

ACKNOWLEDGEMENTS

We are indebted to F. Bussolino, E. Giraudo (IRCC, Candiolo), M. Gasparini, L. Preziosi (Politecnico di Torino) for several fruitful discussions. A. G. thanks I. Kolokolov (Landau Institute, Moscow) and M. Vergassola (CNRS, Nice) for explaining to him their work on the Burgers equation and the adhesion model, and for many stimulating discussions. The authors are indebted to P. Netti (Università di Napoli) for suggesting the introduction of external transport of a chemoattractant. The work was funded by CNR (P.F. Biotecnologie), ISS (Programma Nazionale di Ricerca sull'AIDS: grants 40B.19 and 30B.9; Programma Terapia dei Tumori), MURST cofin and Programmi di Ricerca di Rilevante Interesse Nazionale—1999 and 2000, INdAM-GNFM and the EU RTN 'Using mathematical modelling and computer simulation in cancer therapy'.

REFERENCES

Ambrosi, D. and L. Preziosi (2002). On the closure of mass balance models for tumor growth. *Math. Mod. Meth. Appl. Sci.* **12**, 737–754.

Burgers, J. (1974). *The Non-Linear Diffusion Equation*, D. Reidel Publ. Co.

Byrne, H. M., J. R. King, D. L. S. McElwain and L. Preziosi (2003). *Appl. Math. Lett.* **16**, 567–573.

Carmeliet, P. (2000). Mechanisms of angiogenesis and arteriogenesis. *Nat. Med.* **6**, 389–395.

Cleaver, O. and P. Krieg (1998). VEGF mediates angioblast migration during development of the dorsal aorta in Xenopus. *Development* **125**, 3905–3914.

Di Talia, S., A. Gamba, F. Lamberti and G. Serini. Role of inhibiting factors in mascularization dynamics, in preparation.

Folkman, J. and C. Haudenschild (1980). Angiogenesis in vitro. *Nature* **288**, 551–556.

Fong, G., L. Zhang, D. Bryce and J. Peng (1999). Increased hemangioblast commitment, not vascular disorganization, is the primary defect in *flt-1* knockout mice. *Development* **126**, 3015–3025.

Gamba, A., D. Ambrosi, A. Coniglio, A. de Candia, S. Di Talia, E. Giraudo, G. Serini, L. Preziosi and F. Bussolino (2003). Percolation, morphogenesis, and Burgers dynamics in blood vessels formation. *Phys. Rev. Lett.* **90**, 118101.

Gazit, Y., D. A. Berk, M. Leunig, L. T. Baxter and R. K. Jain (1995). Scale-invariant behavior and vascular network formation in normal and tumor tissue. *Phys. Rev. E* **75**, 2428–2431.

Gengrinovitch, S., B. Berman, G. David, L. Witte, G. Neufeld and D. Ron (1999). Glypican-1 is a VEGF165 binding proteoglycan that acts as an extracellular chaperone for VEGF165. *J. Biol. Chem.* **274**, 10816–10822.

Grant, D., K. Tashiro, B. Segui-Real, Y. Yamada, G. Martin and H. Kleinman (1989). Two different laminin domains mediate the differentiation of human endothelial cells into capillary-like structures in vitro. *Cell* **58**, 933–943.

Gurbatov, S., A. Malakhov and A. Saichev (1991). *Non-Linear Random Waves and Turbulence in Nondispersive Media: Waves, Rays, Particles*, Manchester: Manchester United Press.

Guyton, A. and J. Hall (2000). *Textbook of Medical Physiology*, St. Louis: W.B. Saunders.

Helmlinger, G., M. Endo, N. Ferrara, L. Hlatky and R. Jain (2000). Formation of endothelial cell networks. *Nature* **405**, 139–141.

Hillen, T. and H. Othmer (2000). Chemotaxis equations from the parabolic limit of velocity jump processes. *SIAM J. Appl. Math.* **61**, 751–775.

Holmes, M. and B. Sleeman (2000). A mathematical model of tumor angiogenesis incorporating cellular traction and viscoelastic effects. *J. Theor. Biol.* **202**, 95–112.

Keller, E. F. and L. A. Segel (1970). Initiation of slime mold aggregation viewed as an instability. *J. Theor. Biol.* **26**, 399–415.

Kubota, Y., H. Kleinman, G. Martin and T. Lawley (1988). Role of laminin and basement membrane in the morphological differentiation of human endothelial cells into capillary-like structures. *J. Cell. Biol.* **107**, 1589–1598.

LeVeque, R. (1990). *Numerical Methods for Conservation Laws*, Zurich: Birkhauser.

Manoussaki, D., S. R. Lubkin, R. B. Vernon and J. D. Murray (1996). A mechanical model for the formation of vascular networks *in vitro*. *Acta Biotheor.* **44**, 271–282.

Mardia, K. and P. Jupp (1999). *Directional Statistics*, John Wiley & Sons.

Muller, Y., H. Christinger, B. Keyt and A. de Vos (1997). The crystal structure of vascular endothelial growth factor (VEGF) refined to 1.93 Å resolution: multiple copy flexibility and receptor binding. *Structure* **5**, 1325.

Murray, J. and G. Oster (1984). Cell traction models for generation of pattern and form in morphogenesis. *J. Math. Biol.* **19**, 265–279.

Ngwa, G. and P. Maini (1995). Spatio-temporal patterns in a mechanical model for mesenchymal morphogenesis. *J. Math. Biol.* **33**, 489–520.

Othmer, H. and T. Hillen (2002). Chemotaxis equations from the diffusion limit of transport equations. *SIAM J. Appl. Math.* **62**, 1222–1250.

Othmer, H. and A. Stevens (1997). Aggregation, blowup and collapse: the ABC's of generalized taxis. *SIAM J. Appl. Math.* **57**, 1044–1081.

Pluen, A., P. A. Netti, R. K. Jain and D. A. Berk (1999). Diffusion of macromolecules in agarose gels: comparison of linear and globular configurations. *Biophys. J.* **77**, 542–552.

Richardson, T., M. Peters, A. Ennett and D. Mooney (2001). Functional small-diameter neovessels created using endothelial progenitor cells expanded ex vivo. *Nat. Biotech.* **19**, 1029–1034.

Ruhrberg, C., H. Gerhardt, M. Golding, R. Watson, S. Ioannidou, H. Fujisawa, C. Betsholtz and D. Shima (2002). Spatially restricted patterning cues provided by heparin-binding VEGF-A control blood vessel branching morphogenesis. *Gen. Dev.* **16**, 2684–2698.

Serini, G., D. Ambrosi, E. Giraudo, A. Gamba, L. Preziosi and F. Bussolino (2003). Modeling the early stages of vascular network assembly. *EMBO J.* **22**, 1771–1779.

Shandarin, S. and Y. Zeldovich (1989). The large-scale structure of the universe: turbulence, intermittency, structures in a self-gravitating medium. *Rev. Mod. Phys.* **61**, 185–220.

Stauffer, D. and A. Aharony (1994). *Introduction to Percolation Theory*, London: Taylor & Francis.

Vasiev, B. and C. J. Weijer (1999). Modelling chemotactic cell sorting during Dictyostelium discoideum mound formation. *Biophys. J.* **76**, 595–605.

Velázquez, J. J. L. (2002). Stability of some mechanisms of chemotactic aggregation. *SIAM J. Appl. Math.* **5**, 1581–1633.

Vergassola, M., B. Dubrulle, U. Frisch and A. Noullez (1994). Burgers' equation, devil's staircases and the mass distribution for large-scale structures. *Astron. Astrophys.* **289**, 325–356.

Vernon, R., J. Angello, M.-L. Iruela-Arispe, T. Lane and E.-H. Sage (1992). Reorganization of basement membrane matrices by cellular traction promotes the formation of cellular networks *in vitro*. *Lab. Invest.* **66**, 536–546.

Walter, M., W. Cook, S. Ealick, T. Nagabhushan, P. Trotta and C. Bugg (1992). Three-dimensional structure of recombinant human granulocyte–macrophage colony-stimulating factor. *J. Mol. Biol.* **224**, 1075.

Received 9 June 2003 and accepted 27 April 2004